

## NRC Publications Archive Archives des publications du CNRC

### Numerical simulations of broken ice interaction with structures Barker, Anne; Sayed, Mohamed; Timco, Garry

For the publisher's version, please access the DOI link below./ Pour consulter la version de l'éditeur, utilisez le lien DOI ci-dessous.

#### **Publisher's version / Version de l'éditeur:**

<https://doi.org/10.4224/12328171>

*PERD/CHC Report; no. 9-82, 2000-03*

#### **NRC Publications Archive Record / Notice des Archives des publications du CNRC :**

<https://nrc-publications.canada.ca/eng/view/object/?id=b10a42d8-9526-488c-bc89-a89ec7cf1372>

<https://publications-cnrc.canada.ca/fra/voir/objet/?id=b10a42d8-9526-488c-bc89-a89ec7cf1372>

Access and use of this website and the material on it are subject to the Terms and Conditions set forth at

<https://nrc-publications.canada.ca/eng/copyright>

READ THESE TERMS AND CONDITIONS CAREFULLY BEFORE USING THIS WEBSITE.

L'accès à ce site Web et l'utilisation de son contenu sont assujettis aux conditions présentées dans le site

<https://publications-cnrc.canada.ca/fra/droits>

LISEZ CES CONDITIONS ATTENTIVEMENT AVANT D'UTILISER CE SITE WEB.

**Questions?** Contact the NRC Publications Archive team at

PublicationsArchive-ArchivesPublications@nrc-cnrc.gc.ca. If you wish to email the authors directly, please see the first page of the publication for their contact information.

**Vous avez des questions?** Nous pouvons vous aider. Pour communiquer directement avec un auteur, consultez la première page de la revue dans laquelle son article a été publié afin de trouver ses coordonnées. Si vous n'arrivez pas à les repérer, communiquez avec nous à PublicationsArchive-ArchivesPublications@nrc-cnrc.gc.ca.



**Numerical Simulations of Broken Ice Interaction with Structures**

**Anne Barker, Mohamed Sayed, Garry Timco  
Canadian Hydraulics Centre  
National Research Council of Canada  
Ottawa, Ont. K1A 0R6  
Canada**

**Technical Report HYD-TR-050  
PERD/CHC Report 9-82**

**March 2000**



## ABSTRACT

The interaction of moving broken ice with a structure is an important problem in ice mechanics. Ice-induced loads and pile-ups can result due to this type of interaction, for example, on a bridge pier during spring break-up or on a vessel stationkeeping in pack ice conditions. Numerical techniques can be developed and applied to investigate this type of problem. In this report, a numerical model of ice interaction with both slender and wide structures in varying ice conditions is presented. The model is based on a Particle-In-Cell (PIC) approach, combined with a viscous plastic ice rheology. The plastic yield follows a Mohr-Coulomb criterion. The Zhang-Hibler (1997) numerical scheme is used to solve the momentum equations. The model is used to examine the role of ice thickness, ice properties and velocity on the resulting forces on two different structures. The results show good agreement with the field measurements.

## TABLE OF CONTENTS

ABSTRACT .....	I
TABLE OF CONTENTS .....	II
TABLE OF FIGURES .....	III
1. INTRODUCTION .....	1
2. NUMERICAL MODEL .....	2
2.1 Overview .....	2
2.2 Governing Equations .....	2
2.3 Particle-In-Cell (PIC) Advection .....	5
2.4 Numerical Approach .....	6
2.5 Boundary Conditions .....	7
3. CASE 1: SLENDER STRUCTURE IN CONFINED ICE CONDITIONS.....	9
3.1 Slender Structure .....	9
3.2 Full-Scale Bridge Pier Data .....	9
3.3 Base Case for Slender Structures .....	10
3.4 Parametric Study .....	16
3.5 Comparison with Measurements and Other Calculation Methods.....	18
4. CASE 2: WIDE STRUCTURE IN TIGHT, MANAGED ICE CONDITIONS...20	
4.1 Wide Structure .....	20
4.2 Full-Scale Kulluk Data .....	20
4.3 Base Case for Wide Structure .....	24
4.4 Parametric Study .....	29
4.5 Comparison with Measurements and Other Calculation Methods.....	30
5. SUMMARY .....	31
5.1 Slender Structure in Confined Ice Conditions.....	31
5.2 Wide Structure in Tight, Managed Ice Conditions .....	31
6. ACKNOWLEDGEMENTS .....	32
7. REFERENCES .....	33

## TABLE OF FIGURES

Figure 1 Bridge pier in the White River, Vermont (from Zabilansky, 1996) .....	9
Figure 2 Base grid.....	10
Figure 3 Force-time record for the base case .....	12
Figure 4 Normal stress in x-direction for base case after a) 10 seconds and b) 20 seconds.....	13
Figure 5 Concentration for base case after a) 10 seconds and b) 20 seconds.....	14
Figure 6 Velocity for base case after a) 10 seconds and b) 20 seconds.....	15
Figure 7 Force-time series for different values of $\phi$ .....	16
Figure 8 Force-time series for different values of cohesion .....	17
Figure 9 Force-time series for different ice velocities for base case conditions .....	18
Figure 10 Field measurement load variation for the White River, Vermont (from Zabilansky, 1996).....	19
Figure 11 Illustration of the Kulluk showing its double conical shape and overall features (from Wright, 1999) .....	21
Figure 12 The Kulluk and an ice clearing vessel in thick, managed first-year ice conditions and a schematic of one of the ice-clearing techniques (from Wright, 1999).....	22
Figure 13 Measured loads on the Kulluk in tight managed ice with poor clearance and updrift rubble wedge (from Wright, 1999).....	23
Figure 14 Schematic of updrift rubble wedge at Kulluk in tight pack ice (after Wright, 1999) .....	23
Figure 15 Base grid for Kulluk modelling.....	24
Figure 16 Initial ice concentration profile around the Kulluk.....	25
Figure 17 The effect of $\phi$ on numerical peak load .....	26
Figure 18 Rubble wedge build-up in tight pack ice conditions, updrift of the Kulluk (from Wright, 1999) .....	26
Figure 19 Ice concentration profile around Kulluk showing the ice build-up in front of the Kulluk after a) 150 s and b) 300 s from the start of the run.....	27
Figure 20 Pressure profiles around the Kulluk after a) 150 s and b) 300 s from the start of the run .....	28
Figure 21 Velocity profiles around the Kulluk after a) 150 s and b) 300 s from the start of the run .....	29
Figure 22 Numerical load versus initial ice thickness, for $\phi=27^\circ$ , $c=0.95$ .....	30



# NUMERICAL SIMULATIONS OF BROKEN ICE INTERACTION WITH STRUCTURES

## 1. INTRODUCTION

Broken ice is abundant in nature. Movement of broken ice due to environmental driving forces can lead to ice loads on coastal and offshore structures. For example, in the offshore regions, broken ice can exert forces on fixed and floating structures. For most cases in offshore regions, these forces are not design level ice forces, especially for bottom-founded structures. However, for floating structures, such as the Kulluk that was used in the Beaufort Sea, or the FPSO that will be used in the Grand Banks region, forces due to pack ice must be considered. In these cases, it is important to ensure that the ice-induced loads do not exceed the mooring line capacity of the vessel. In spite of its importance, there is only limited knowledge of the load levels that can be exerted by moving broken ice.

This report develops a numerical model that can be used to predict these forces. The model is based on a model developed earlier for ice forecasting (Sayed and Carrieres, 1999). This two-dimensional numerical model, which uses a “Particle in Cell” approach, has been modified to study pack ice forces on wide offshore structures (Sayed et al., 2000). The full details of the model is presented and discussed in Chapter 2.

Two different full-scale situations are used to calibrate and verify the model. The first case concerns ice interacting with a slender structure and it is described in Chapter 3. Model results for that case are verified using field measurements of broken river ice impact on a bridge pier during spring break-up. The second case models the floating vessel “Kulluk” which was used in a moored mode in the exploration of the Beaufort Sea. In this case, there was tightly managed ice interacting with a wide floating structure (Chapter 4). The details for each case study are presented and the resulting forces and behaviour of the ice cover are examined. The results are then compared to field measurements and other calculation methods.

The emphasis of the present work is the examination of the appropriate choice of material properties, predicting forces on different structures, and verification of the numerical results.

## 2. NUMERICAL MODEL

### 2.1 Overview

For the Particle-In-Cell (PIC) approach, the ice cover is conceptually represented by discrete particles that are individually advected. The term *advection* is used here to refer to integrating a particle's velocity with respect to time, thus determining the new position (or coordinates). Particles are used to model advection in a Lagrangian manner. The momentum equations, however, are solved over a fixed (or Eulerian) grid. Therefore, the approach can be viewed as a hybrid method. Continuum equations are also used to describe the rheology of the ice.

In the two-dimensional formulation, each particle is considered to have an area and a volume. The area of a particle can decrease if the pressure exceeds a certain limit (i.e. ridging pressure). The volume, however, remains constant. Thus, if a particle is subjected to relatively high pressures, its area may decrease, and its thickness would correspondingly increase (constant volume = area x thickness). Note that the particles are not actual ice floes, but computational constructs.

At each time step, the areas of the particles are *mapped* to a fixed grid; i.e. the areas of the particles are converted to continuum ice concentration values (area of ice/ total area) for each cell of the grid. Similarly, the thicknesses of the particles are converted to continuum ice thickness values at the cells of the grid. Such mapping from the particles to the fixed grid is done using a *weighting function*. Thus, when calculating ice concentration for a cell in the fixed grid, particles closer to the cell centre are given higher weight than those farther away.

Once values of ice concentration and thickness are determined over the fixed grid, the continuum momentum and rheology equations are solved over that grid. The use of a fixed grid makes it possible to employ *implicit* numerical methods, which are efficient. The time steps can be very large compared to explicit formulations that must be used, for example, in discrete element methods. In the present model, the numerical method of Zhang and Hibler (1997) is used because of its efficiency.

The solution of the momentum and rheology equations gives velocity values at the nodes of the fixed grid. Those velocities are mapped from the nodes to the particles in a manner similar to that discussed above. The particles are then advected to new positions.

### 2.2 Governing Equations

The governing equations consist of:

- Continuum linear momentum equations.

- Continuum rheology, which is represented here by a viscous plastic model of Mohr-Coulomb yield criterion.
- Mapping functions to convert particles' areas and thicknesses to continuum values on the fixed grid, and to convert velocities at the grid nodes to velocities for each particle.

The momentum equations are expressed as

$$mass_{ice} \frac{d\vec{u}}{dt} = \nabla \cdot \sigma + \vec{\tau}_a + \vec{\tau}_w \quad (2.1)$$

where  $mass_{ice}$  is the mass of the ice cover per unit area ( $mass_{ice} = \rho_{ice} h$ ),  $\rho_{ice}$  is ice density,  $h$  is the ice thickness,  $\vec{u}$  is the velocity vector,  $\sigma$  is the stress tensor, and  $\vec{\tau}_a$  and  $\vec{\tau}_w$  are the air and water drag stresses. The air and water drag stresses are given by the following quadratic formulas

$$\vec{\tau}_a = c_a \rho_a |\vec{U}_a| \vec{U}_a \quad (2.2)$$

and

$$\vec{\tau}_w = c_w \rho_w |\vec{U}_w - \vec{u}| (\vec{U}_w - \vec{u}) \quad (2.3)$$

where  $c_a$  and  $c_w$  are the air and water drag coefficients,  $\vec{U}_a$  is wind velocity,  $\vec{U}_w$  is water velocity, and  $\rho_a$  and  $\rho_w$  are the air and water densities, respectively. Eq.(2.2) assumes that ice velocity is small compared to wind velocity.

The stress-strain rate relationship is given by

$$\sigma_{ij} = -p \delta_{ij} + 2\eta \dot{\varepsilon}_{ij} + (\zeta - \eta) \dot{\varepsilon}_{kk} \delta_{ij} \quad (2.4)$$

where  $\dot{\varepsilon}_{ij}$  is the strain rate,  $p$  is the mean normal stress,  $\eta$  is the shear viscosity, and  $\zeta$  is the bulk viscosity. Note that  $\dot{\varepsilon}_{kk}$  is the volumetric strain rate. The bulk viscosity,  $\zeta$ , is difficult to measure or infer because relatively large rates of change of density must be used. It is common, however, to assume that either  $(\zeta - \eta)$  or  $\zeta$  is negligible. It is assumed here that the bulk viscosity,  $\zeta$ , is zero. An advantage of this assumption is that the resulting ratio between the principal stresses agrees with the Mohr-Coulomb criterion.

The mean normal stress,  $p$ , is usually considered to increase with increasing ice concentration,  $A$  (area of ice/total area). Here, a formula analogous to that of Hibler (1979) is used. Note, however, that  $p$  is defined according to the common convention in

continuum mechanics literature, and is different from the strength  $P$  used by Hibler (1979) by a factor of two.

$$p = P^* h_{ice} \exp(-K(1-A)) \quad (2.5)$$

where  $P^*$  is a reference ice strength, and  $K$  is a constant.

Equation (2.5) is convenient for use with intact ice sheets or pack ice with little vertical confinement (due to buoyancy), since ice cover strength (per unit length) would be proportional to the thickness,  $h_{ice}$ . For the case of ice covers consisting of bulk rubble, however, strength of the ice cover would be proportional to the vertical confining pressure. It is straightforward to see that the vertical confining pressure is proportional to the buoyancy of the ice rubble (and therefore proportional to  $h_{ice}^2$ ). For those cases, the mean normal stress is expressed as

$$p = P^* h_{ice}^2 \exp(-K(1-A)) \quad (2.6)$$

The Mohr-Coulomb criterion is introduced by giving the shear viscosity,  $\eta$ , the following value

$$\eta = \frac{(c \cot \phi + p) \sin \phi}{\Delta} \quad (2.7)$$

where  $\phi$  is the angle of internal friction, and  $c$  is the cohesion. The strain rate  $\Delta$  is given by

$$\Delta = \max(|\dot{\varepsilon}_1 - \dot{\varepsilon}_2|, \dot{\varepsilon}_0) \quad (2.8)$$

where  $\dot{\varepsilon}_1$  and  $\dot{\varepsilon}_2$  are the principal strain rates and  $\dot{\varepsilon}_0$  is a threshold strain rate. For relatively large strain rates,  $\Delta > \dot{\varepsilon}_0$ , the rheology is plastic and the yield criterion is satisfied. At small rates of deformation, however, the shear viscosity becomes constant, and the corresponding rheology would be viscous. A very small threshold strain rate is used in order to maintain a predominantly plastic deformation.

The value of  $\dot{\varepsilon}_0$  was chosen by testing a range of values. Using smaller values did not produce any noticeable differences in the results. This indicates that deformation was predominantly plastic. In this analysis, a value of  $10^{-20} \text{ s}^{-1}$  was used as the threshold strain rate. This value is also commensurate with that used by Hibler (1979), albeit for larger geophysical length scale. Nonetheless, it should not be extrapolated to other problems without ensuring that it is sufficiently small.

The preceding set of equations, together with PIC advection, is sufficient to determine the stresses, velocities, and configuration of the ice cover through its interaction with a structure.

### 2.3 Particle-In-Cell (PIC) Advection

In the PIC formulation, the ice cover is discretized into individual particles that are advected in a Lagrangian manner. Each particle is considered to have an area and a thickness. For each time step, the particle velocities are determined by interpolating node velocities of an Eulerian grid. Particles can then be advected. The area and mass of each particle are then interpolated back to update the thickness and ice concentration at the Eulerian grid nodes.

A bilinear interpolation function is used to map variables between the particles and the Eulerian grid. For a particle  $n$  at location  $x_p, y_p$ , and grid node co-ordinates  $(x_{ij}, y_{ij})$ , the interpolation coefficients  $\omega$  would be given by

$$\omega_x(x_{ij}, x_p(n, t)) = [\Delta x - |x_p(n, t) - x_{ij}|] \frac{S_x(i, j, n)}{\Delta x}$$

$$S_x(i, j, n) = \begin{cases} 1 & \text{if } |x_p(n, t) - x_{ij}| \leq \Delta x \\ 0 & \text{otherwise} \end{cases} \quad (2.9)$$

and

$$\omega_y(x_{ij}, x_p(n, t)) = [\Delta y - |y_p(n, t) - y_{ij}|] \frac{S_y(i, j, n)}{\Delta y}$$

$$S_y(i, j, n) = \begin{cases} 1 & \text{if } |y_p(n, t) - y_{ij}| \leq \Delta y \\ 0 & \text{otherwise} \end{cases} \quad (2.10)$$

where  $t$  is time, and  $\Delta x$  and  $\Delta y$  are the grid cell dimensions.

Thus, the particle velocity components,  $u_p$  and  $v_p$  can be calculated as follows

$$u_p(X(n, t)) = \sum_i \sum_j \omega_x(x_{ij}, x_p(n, t)) \omega_y(y_{ij}, y_p(n, t)) u(i, j),$$

$$v_p(X(n, t)) = \sum_i \sum_j \omega_x(x_{ij}, x_p(n, t)) \omega_y(y_{ij}, y_p(n, t)) v(i, j) \quad (2.11)$$

where  $u(i, j)$  and  $v(i, j)$  are the velocity components of the Eulerian velocity grid.

Once particles' velocities are determined, advection of a particle,  $n$  at location  $\mathbf{X}$ , can be expressed as

$$\mathbf{X}(n, t + \Delta t) = \mathbf{X}(n, t) + \int_t^{t+\Delta t} \mathbf{u}(\mathbf{X}(n, t'), t') dt' \quad (2.12)$$

where  $\mathbf{u}$  is the particle's velocity vector and  $\Delta t$  is the time step. The integral in Eq. (2.12) can be approximated by

$$\int_t^{t+\Delta t} \mathbf{u}(\mathbf{X}(n, t'), t') dt' = \mathbf{u}(\mathbf{X}^*(n, t)) \Delta t,$$

$$\mathbf{X}^* = \mathbf{X}(n, t) + \mathbf{u}(\mathbf{X}(n, t), t) \frac{\Delta t}{2} \quad (2.13)$$

The updated thickness and concentration are determined at each time step by mapping particles' areas and volumes back to the Eulerian grid. The values of node concentration  $c(x_{ij}, t)$  are determined as follows

$$c(x_{ij}, t) = \sum_n \omega_x(x_{ij}, \mathbf{X}(n, t)) \omega_y(x_{ij}, \mathbf{X}(n, t)) A(n, t) \frac{1}{\Delta x \Delta y} \quad (2.14)$$

where  $A(n, t)$  is the area of particle  $n$ . The values of node thickness are then calculated as follows

$$h(x_{ij}, t) = \sum_n \omega_x(x_{ij}, \mathbf{X}(n, t)) \omega_y(x_{ij}, \mathbf{X}(n, t)) V(n, t) \frac{1}{c(x_{ij}, t) \Delta x \Delta y} \quad (2.15)$$

where  $V(n, t)$  is the volume of particle  $n$ .

The resulting concentration and thickness are further modified to account for ridging, which may occur if the ice cover converges. If the concentration at a node, according to Eq. (2.14), is larger than unity, its value is adjusted to one. The thickness at that node is also increased to conserve the volume of ice. Such a correction of concentration and thickness is mapped back to the particles.

## 2.4 Numerical Approach

The solution is implemented using a staggered grid. The velocity components are defined at the corners of the velocity grid. All scalar values (pressure, viscosities, thickness and concentration) are defined at the centres of the grid cells.

Starting from a given initial configuration, the numerical solution of the above governing equations updates the velocities, pressures, thicknesses, and concentrations at each time step. The main logic of the solution consists of the following steps:

- Advect the particles to new positions.
- Determine the thickness and concentration values by interpolating the area and volume of the particles to the scalar grid.
- Correct the thickness and concentration values by adjusting concentrations higher than unity. Next, correct the area and thickness of each particle.
- Calculate the pressures on the scalar grid using Eq.(2.5).

- Solve the momentum equations Eq.(2.1). The numerical approach is briefly discussed below.
- Determine particle velocities by interpolating values from the velocity.

A brief overview of the implicit solution of momentum equations is presented here (for details, see Zhang and Hibler, 1997). The basic idea is to uncouple the x and y components of the momentum equations, and to linearize the terms involving water drag and ice stress by using velocity values from the previous time step. Furthermore, an iteration loop is added to ensure that the plastic yield conditions are satisfied. In the present implementation, advection terms are included (which were not considered by Zhang and Hibler, 1997) by using velocities from the previous time step.

The method is illustrated by considering the x-component momentum equation. The solution consists of two levels. In the 1<sup>st</sup> level, a first estimate of the velocity is obtained from

$$\begin{aligned}
 & mass_{ice} \frac{u_1^{n+1} - u_1^n}{\Delta t} - \partial_x [\eta \partial_x u_1^{n+1}] - \partial_y [\eta \partial_y u_1^{n+1}] + c_w \rho_w |U_w - \mathbf{u}^n| u_1^{n+1} \\
 & = \tau_{air-x} - \partial_x [\eta \partial_y v^n] + \partial_y [\eta \partial_x u^n] + c_w \rho_w |U_w - \mathbf{u}^n| U_{wx} \\
 & \quad - \partial_x p - u^n \partial_x u^n - v^n \partial_y u^n
 \end{aligned} \tag{2.16}$$

where the superscripts  $n$  and  $n+1$  refer to time steps  $n$  and  $n+1$  respectively. Note that  $u$  and  $v$  are the x and y components of the velocity vector,  $\mathbf{u}$ . The subscript 1 refers to the 1<sup>st</sup> level, and the viscosity coefficient  $\eta$  is evaluated using  $\mathbf{u}^n$ . The x- components of air drag stress and water velocity are  $\tau_{air-x}$  and  $U_{wx}$ , respectively.

In the 2<sup>nd</sup> level of the solution, the x-component velocity  $u^{n+1}$  is evaluated using an equation similar to Eq. (2.15), but using updated values of  $\eta$  that are calculated using velocities  $\mathbf{u}^c$

$$\mathbf{u}^c = (\mathbf{u}_1^{n+1} + \mathbf{u}^n) / 2 \tag{2.17}$$

The spatial derivatives in Eq. (2.16) are evaluated using central difference formulas (e.g. Hibler, 1979). Thus the left-hand side of Eq. (2.16) would have 3 unknown velocities at time step  $n+1$ . The solution of Eq. (2.16) is done using point successive over relaxation. The solution of both the 1<sup>st</sup> and 2<sup>nd</sup> levels is repeated in an iteration loop, called pseudo time stepping, while updating the viscosity coefficient,  $\eta$ . The iteration loop ensures that the plastic yield condition is satisfied.

## 2.5 Boundary Conditions

A *no-slip* boundary condition can be implemented via a mask, setting velocities to zero for all nodes within the structure or fixed boundary. Additionally, a *full-slip* condition may

be implemented by preventing particles from moving through the boundaries, but allowing them to move in a parallel direction. For example, to implement a full-slip condition at the top boundary of the grid if a particle moved upward through the boundary, its y-position is reset to a value immediately below the boundary or immediately above the opposite boundary, without changing its x-position.

The PIC approach does not require imposing conditions at the free interface between the ice cover and open water (e.g. leads). At such interfaces, the particles can move according to the governing equations, and the free interface evolves. It is important, however, to use the appropriate velocity values at open water nodes since they influence both the solution of the momentum equations and velocity interpolation from the grid to the particles. The approach used in the present study was to solve the momentum equations over all open water nodes. This procedure requires introducing a minimum value of ice thickness at such nodes to avoid numerical problems.

This model has been used to study ice interaction with both slender structures (Section 3) and wide structures (Section 4).

### 3. CASE 1: SLENDER STRUCTURE IN CONFINED ICE CONDITIONS

#### 3.1 *Slender Structure*

Estimates of ice forces on bridge piers involve uncertainties, which motivated several field measurements and numerical studies. There have been a number of field investigations to measure the impact loads on a bridge pier with moving broken river ice. Recently, Johnston et al. (1999) presented an overview and analysis of available data, including the measurements at Hondo, Pembridge, Rideau and St. Regis Rivers piers. Numerical simulations of river ice interaction with hydraulic structures include a discrete element formulation by Daly and Hopkins (1998). Lu and Shen (1998) used both a viscous plastic and an elastic viscous plastic continuum rheology to model river ice transport.

Simulation runs for this case focused on a single slender pier geometry, consisting of a rectangular shape with a circular front. Zabilansky (1996) reported on detailed measurements of ice forces on such a pier in the White River (see Figure 1). His measurements, along with similar measurements made by Sodhi et al. (1983), are used to verify the numerical results. The description of these test sites is outlined in the following sub-section. The numerical model that corresponds to this case and comparison with the field measurements follows the description of the test sites.



**Figure 1 Bridge pier in the White River, Vermont (from Zabilansky, 1996)**

#### 3.2 *Full-Scale Bridge Pier Data*

Zabilansky (1996) reported on measurements made on the White River in Vermont. In this case, the pier width was circular with a 1.22 m diameter and a 15° inclination. The river ice during the break-up run was about 0.25 to 0.45 m thick, with floe sizes ranging up to 5 m. The ice was in a single layer (i.e. no rafting) and of high concentration (0.75 to 0.95 coverage). Zabilansky reported maximum loads of 0.12 MN, with typical peak loads on the order of 0.04 to 0.06 MN.

Sodhi et al (1983) reported on measurements of river ice interacting with a bridge pier on the Ottawaquechee River in Vermont. In this case, the pier was vertical and 0.61 m wide with a V-shape. They reported a river ice run with floe sizes on the order of 1 to 10m, with a thickness range of 0.15 m to 0.6 m. The maximum load was reported to be 0.12 MN, with a high static load of 0.11 MN. In this case, however, the static load occurred due to bridging of the ice floes between the pier and the shoreline.

### 3.3 Base Case for Slender Structures

Figure 2 shows a schematic of the numerical grid and the pier. A 200- by 85-node grid represents the study area. The grid cell size is 0.3 m. The grid thus covers 60 m along the length of the river, and 25.5 m across the width. The pier instrumented by Zabilansky (1996) was 1.22 m wide, which is represented over a width of approximately 4 nodes. Full slip boundary conditions were used at the top and bottom of the grid, which represent riverbanks. If a particle moved, for example, through the top boundary, its y-position would be changed to bring it back within the grid without changing its x-position. A no slip boundary condition was used for the pier. Velocities of the nodes within the pier were set to zeros. Additionally, if a particle crossed the boundary of the pier, its normal displacement was reset to zero. The latter procedure accounted for the circular shape of the pier. Note that just fixing node velocities to zeros would produce a step-like boundary for the pier instead of a circular one.

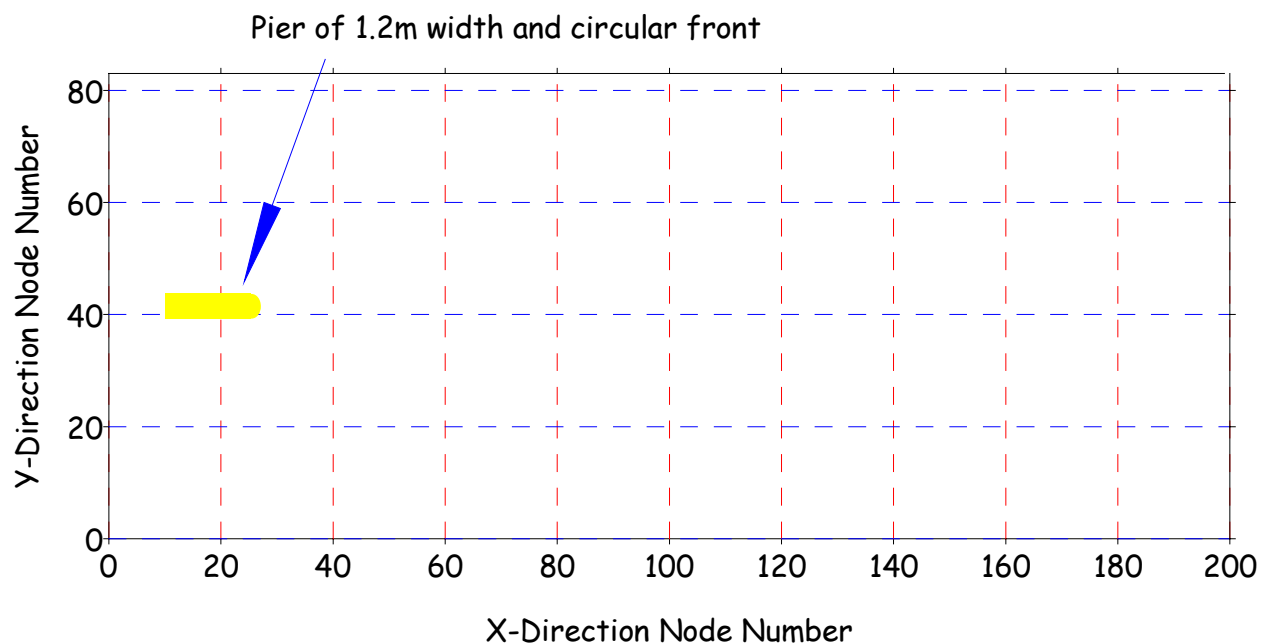


**Figure 2 Base grid**

The ice cover was driven against the pier by imposing a constant velocity upstream. The constant driving velocity was applied to a 36 m wide zone at the upstream side

(node number 80 to 200 along the x-direction, Figure 2). The relatively large size of that zone ensured that a sufficient supply of particles would flow against the structure during the runs. A 7 m wide part of the grid adjacent to the downstream boundary was initialized with no ice. This allowed the ice cover to move freely past the pier, without interference from the downstream edge of the grid.

Simulations were chosen to cover a range of plausible ice properties and other parameter values. Compressibility of the ice cover was introduced by using Eq. (2.6). A cohesive Mohr-Coulomb criterion was also used. The role of ice properties was examined by varying the cohesion,  $c$ , angle of internal friction,  $\phi$ , and compressive strength parameter,  $P^*$ . Several values of ice velocities and initial ice concentration were also used. In addition, preliminary runs examined the effect of grid cell size, number of grid nodes, and size of the time step. Those preliminary tests ensured that the chosen grid and time step did not introduce spurious numerical effects.

As an example, the results of the base case are presented here. The parameters used for that case were:

- Angle of internal friction,  $\phi = 45^\circ$ .
- Cohesion,  $c = 50$  kPa.
- Compressive stress parameter,  $P^*$  (Eq. 2.6) = 100 kPa.
- Ice velocity = 0.5 m/s.
- Ice thickness = 0.3 m.
- Drag coefficient = 0.005.
- Time step = 0.1 s.

The resulting force on the pier is plotted versus time in Figure 3. The force was estimated by summing the stress (along the x-direction) and multiplying this by grid cell length for the grid cells immediately in front (upstream) of the pier. The lateral force on the pier was negligible. The force shown in Figure 3 reaches a maximum after approximately 17 s. A number of runs were done for different durations and grid sizes and showed that the force remains at that maximum value.

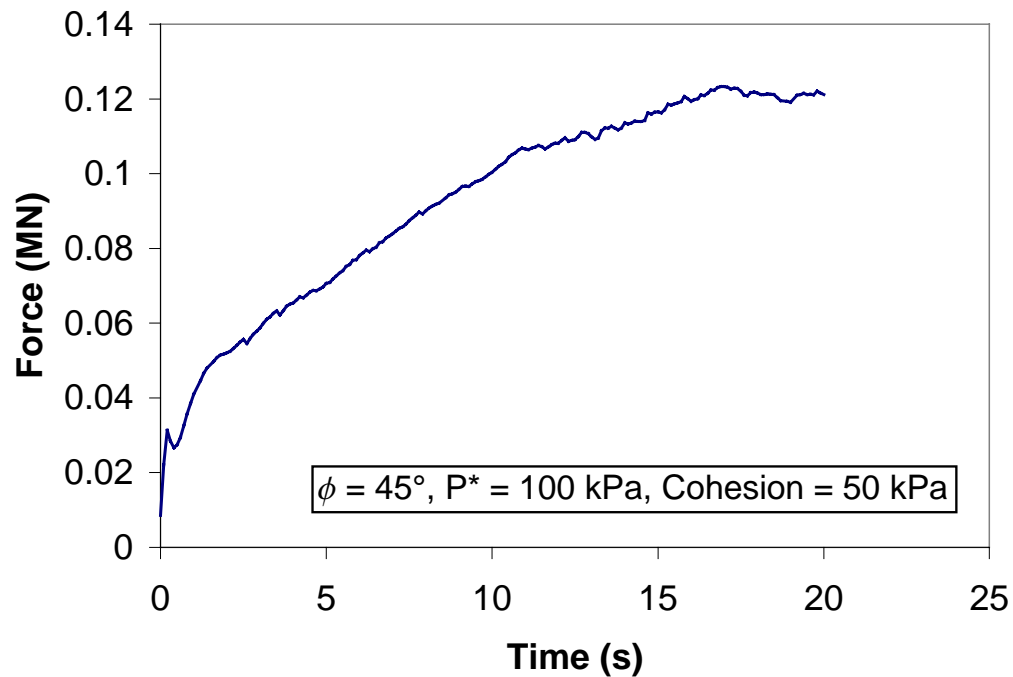
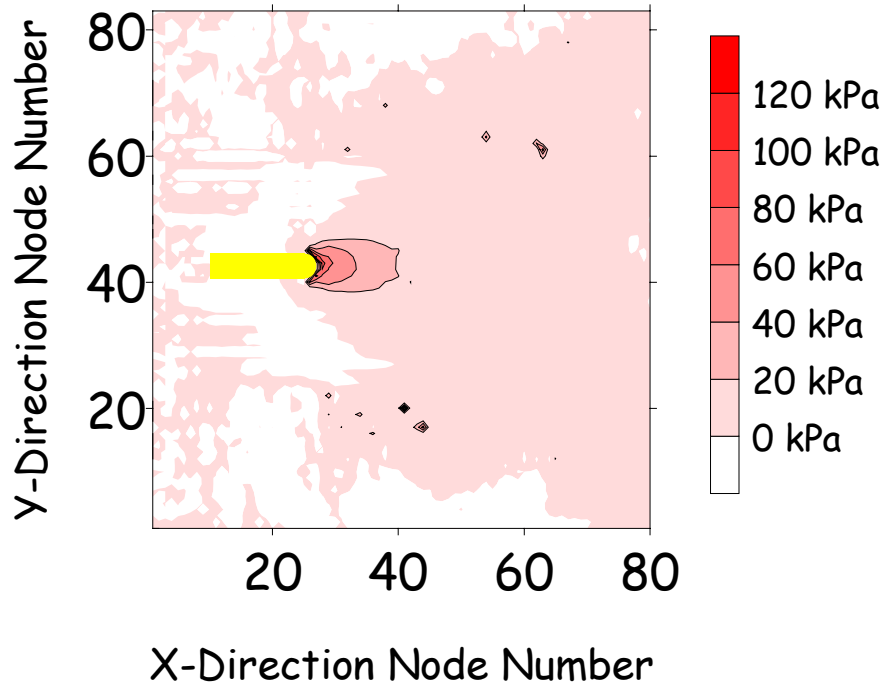


**Figure 3 Force-time record for the base case**

Contours of the normal stress in the x-direction and ice concentration are shown in Figure 4 and Figure 5, respectively. These plots, zoomed in to highlight the portion of the grid nearest the pier, show snapshots after approximately 10 s and 20 s from the start of the run, which is slightly before, and then after, the occurrence of the maximum force. The normal stress contours show higher values in a bulb-shaped zone in front of the pier, as would be expected. Concentration contours display a similar pattern, with high values in front of the pier. A concentration of one (full ice coverage) is evident in the high-pressure zone. There was no noticeable thickness build-up for the base run. This indicated that the compressive strength of the ice cover was relatively high. A weaker strength (lower  $P^*$ ) would cause an increase of ice thickness in high-pressure zones (see, for example, Sayed et al. 2000).

a)



b)

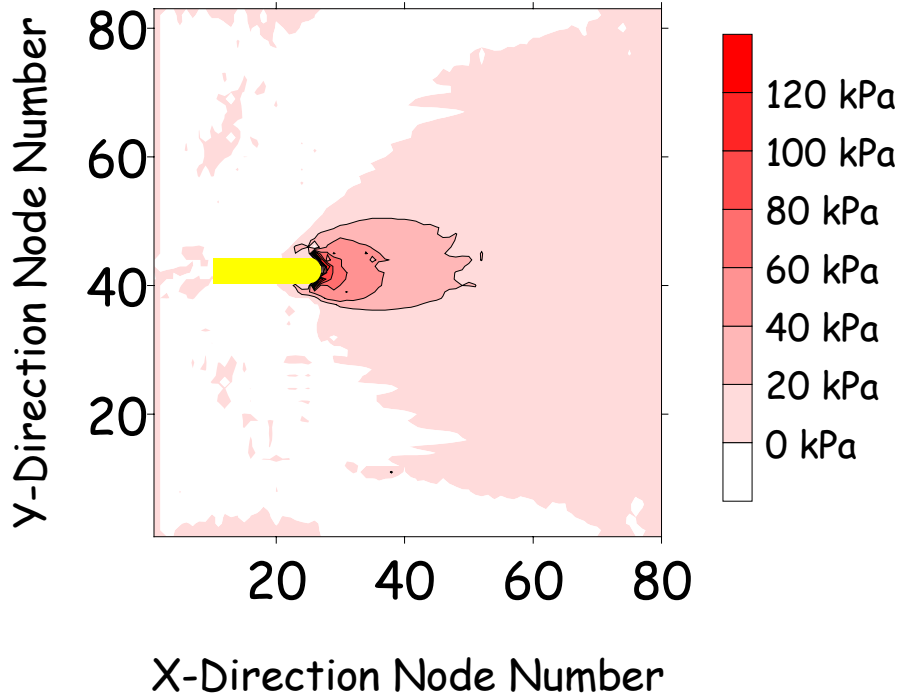
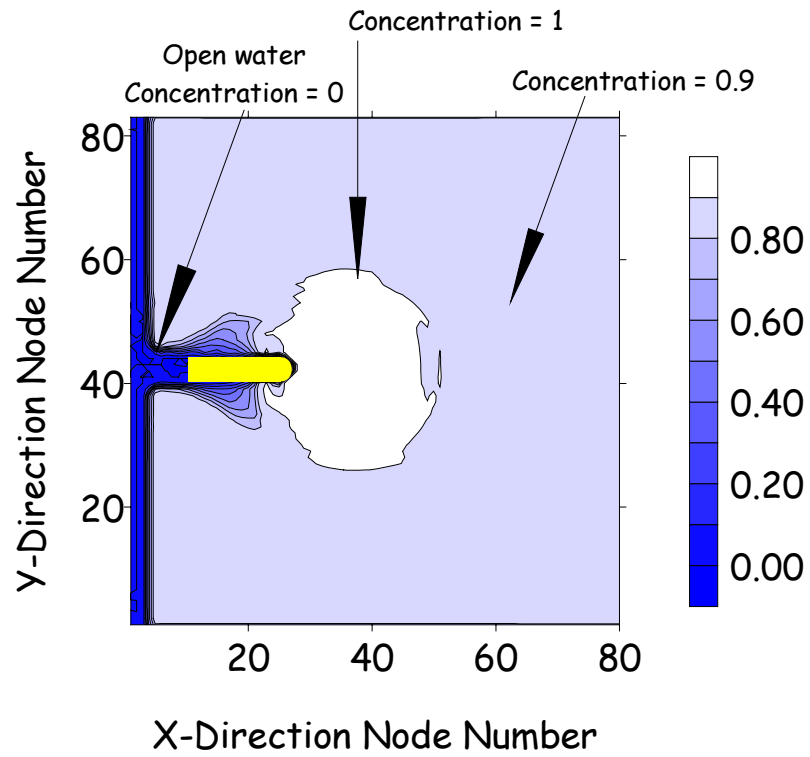


Figure 4 Normal stress in x-direction for base case after a) 10 seconds and b) 20 seconds

a)



b)

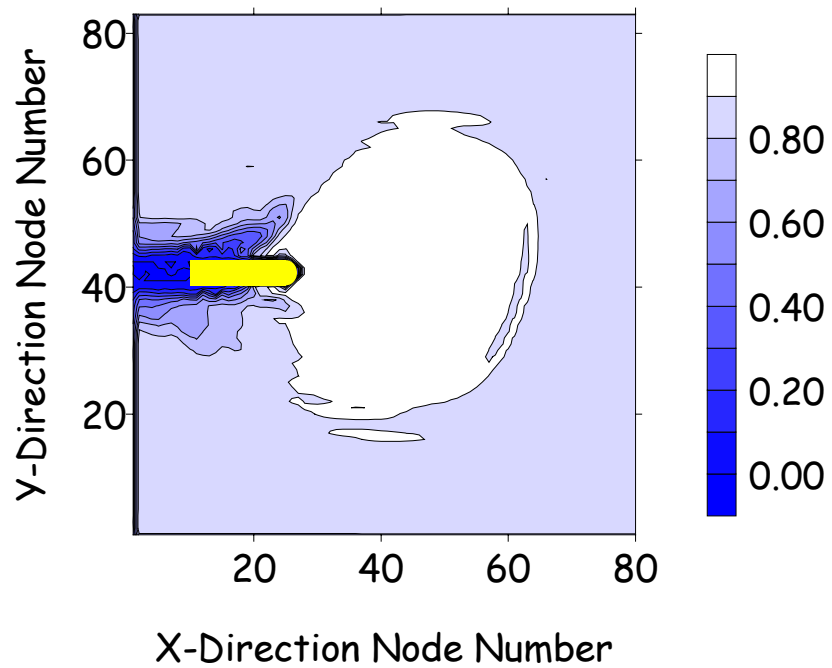
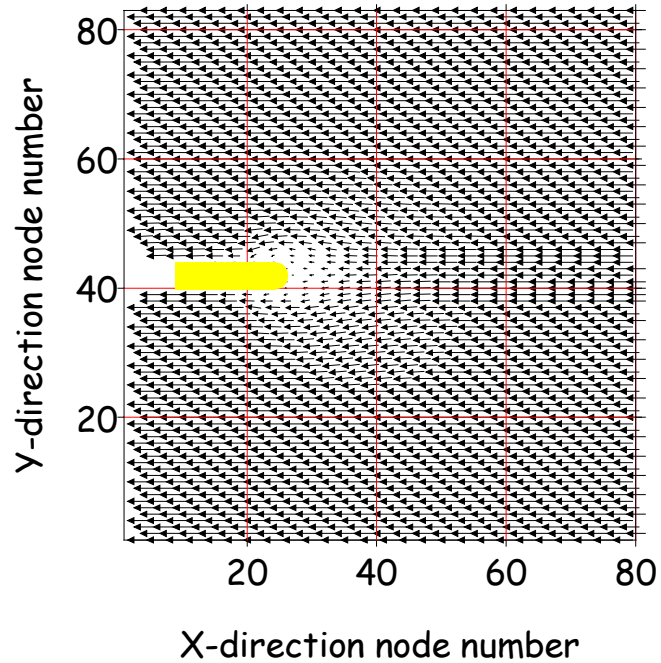


Figure 5 Concentration for base case after a) 10 seconds and b) 20 seconds

Velocity vectors, which correspond to the above stress and concentration results, are plotted in Figure 6. They show the expected behaviour of uniform values and direction away from the pier. The ice cover velocity, however, slows in front of the pier.

a)



b)

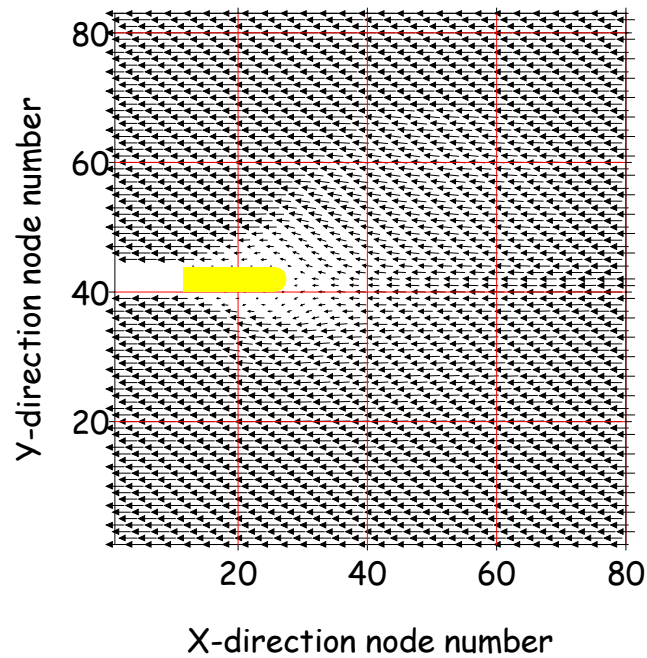


Figure 6 Velocity for base case after a) 10 seconds and b) 20 seconds

### 3.4 Parametric Study

In addition to the base case, a parametric study was carried out. The purpose was to determine the sensitivity of the predicted forces to various factors and parameters, and to determine the appropriate parameter values that may lead to agreement with field measurements.

Although there have been a number of laboratory studies investigating the behaviour of ice rubble, to the authors' knowledge, there have not been any measurements made of the mechanical properties of loose, broken ice floes. Thus, in the present case, the model could not use independently derived, mechanical properties. Instead, the range of values chosen for  $c$  and  $\phi$  in these runs are in the range quoted for ice rubble (e.g. Ettema and Urroz-Aguirre, 1991).

The effect of a suitable range of values for the angle of internal friction,  $\phi$ , is illustrated in Figure 7, where force on the pier is plotted versus time. A similar plot for a range of cohesion values,  $c$ , is shown in Figure 8. All other variables remained the same as those of the base case.

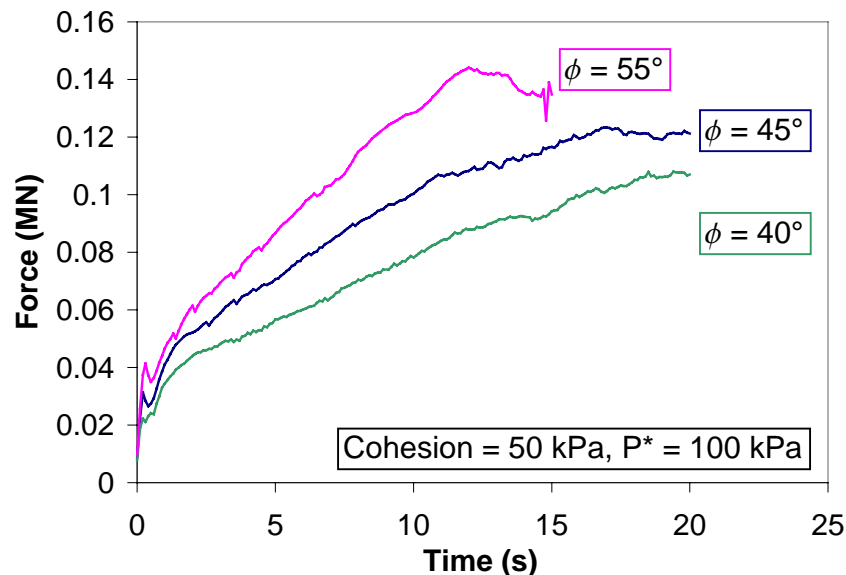
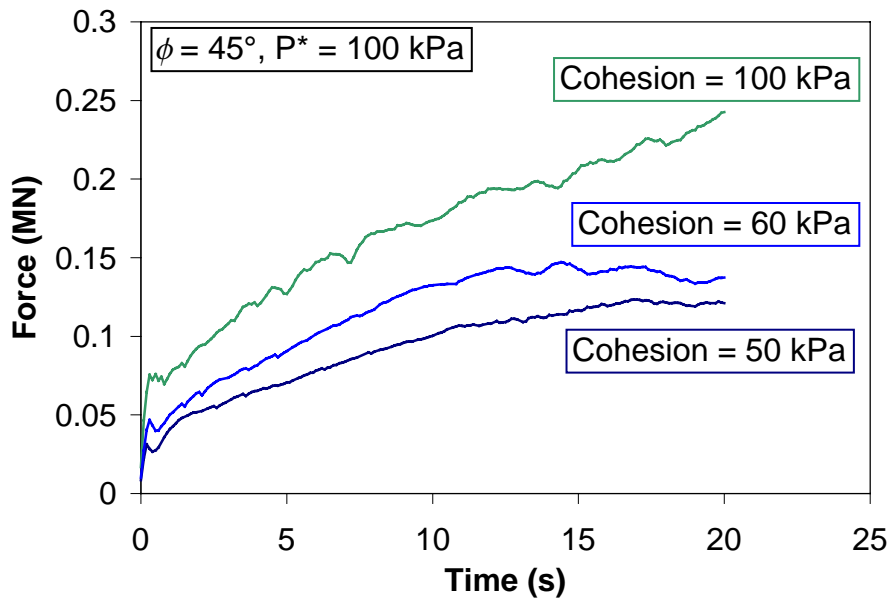


Figure 7 Force-time series for different values of  $\phi$



**Figure 8 Force-time series for different values of cohesion**

The results shown in Figure 7 and Figure 8 indicate that the cohesion has a considerable influence on the predicted force, within the range of chosen values. The peak force values range from 0.03 MN for zero cohesion to a value of 0.15 MN for a cohesion value of 60 kPa. The angle of internal friction,  $\phi$ , has less influence on the force. The maximum force varied from 0.105 MN for  $\phi = 40^\circ$ , to 0.142 MN for  $\phi = 55^\circ$ .

The role of ice velocity was examined by testing values ranging from 0.1 m/s to 0.5 m/s. The resulting forces are plotted versus time in Figure 9. Somewhat surprisingly, ice velocity shows minor influence on the maximum force. This result may be explained by viewing the plot of velocity vectors in Figure 6. It indicates that ice decelerates in a relatively small zone in front of the pier. Therefore the inertia effects of the moving ice would be small for the relatively narrow pier considered here. It should be noted, however, that this result should not be extrapolated to wide structures where the inertia of the ice cover may have more significant effects.

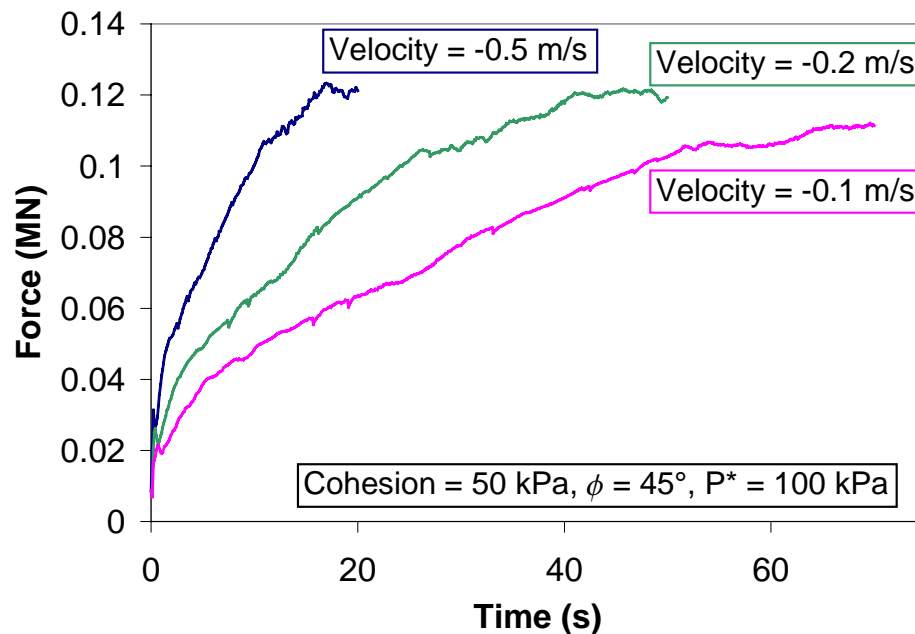


**Figure 9 Force-time series for different ice velocities for base case conditions**

### 3.5 Comparison with Measurements and Other Calculation Methods

The peak loads reported by Sodhi et al. (1983) and Zabilansky (1996) of approximately 0.12 MN are in very good agreement with the loads predicted using the present model (see Figure 3 for the base case). A good correlation between the present model and the reported peak measurements in full-scale tests was found using a cohesion value of 50 kPa and a  $\phi$  value of  $45^\circ$ . It should be noted that the comparison in this case is directed towards the *peak* load measured during the field experiments. The time-series behaviour of the loading events is quite different for the two situations. In the numerical model, the load monotonically rises to a plateau value representing the peak value for the load (again, see Figure 3). In the field measurements, the load variation is much more dynamic, as it represents numerous individual impact events (see Figure 10). The numerical model essentially integrates the individual impacts to represent a continuum approach.

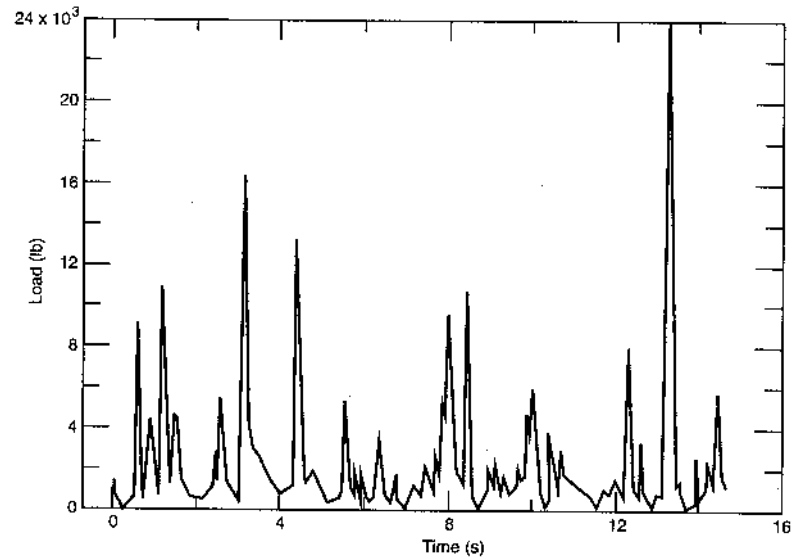


**Figure 10 Field measurement load variation for the White River, Vermont (from Zabilansky, 1996)**

The conventional approach for calculating ice loads during dynamic loading events is to use a modified Korzhavin equation (Korzhavin, 1971). The force ( $F$ ) on the pier is given by

$$F = m I D h \sigma_o \quad (3.1)$$

where  $m$  is a shape factor ( $=0.9$  for a circular pier),  $I$  is the indentation factor,  $D$  is the pier width,  $h$  is the ice thickness and  $\sigma_o$  is the nominal strength value. The original Korzhavin equation also includes a contact factor, but for impact loading, this coefficient is combined with the Indentation factor. Afanasev (1973) has given the combined Indentation coefficient as

$$I = (5 h / D + 1)^{0.5} \quad (3.2)$$

for aspect ratios ( $D/h$ ) less than 6. Sodhi et al. (1983) measured the compressive strength of the ice and report values in the range of 1.6 to 2.7 MPa. Assuming this strength range is appropriate for the White River ice, and using suitable values for pier width and maximum ice thickness, the calculated force on the White River pier is on the order of 1.5 to 2 MN. This load level is significantly higher than the measured peak value of 0.12 MN reported by Zabilansky (1996). This large difference probably reflects the fact that the Korzhavin approach assumes full ice crushing due to the interaction. Although this may be true with large ice floes, continuous crushing does not usually occur in the smaller ice floes encountered here.

## **4. CASE 2: WIDE STRUCTURE IN TIGHT, MANAGED ICE CONDITIONS**

### **4.1 *Wide Structure***

The “Kulluk” was a conical drilling unit that was used for exploratory drilling in the intermediate to deeper waters (20m - 50m) of the Beaufort Sea during the 1980’s and early 1990’s. It was designed as a “second generation” drilling system to significantly extend the open water season, by beginning drilling operations in the spring break-up period and continuing until early winter. It drilled twelve wells at a variety of locations.

During its deployment in the Beaufort Sea, it was exposed to a wide range of moving pack ice conditions. This is the only moored vessel, on a worldwide basis, that has stationkept in a “near full spectrum” of pack ice, from low concentrations of thin ice to high concentrations of rough first-year and multi-year ice. The loads on the mooring lines were monitored and this information provides a unique data set of the forces of a moored vessel in pack ice conditions (Wright 1999).

Stationkeeping in moving pack ice is an important area of ice engineering in many different applications. For example, on the East Coast of Canada, the Terra Nova development will soon begin using a Floating Production Storage and Offloading (FPSO) system that will have to stationkeep, on occasion, in moving pack ice conditions. In other ice-covered regions such as the Beaufort Sea, the Pechora Sea and offshore Sakhalin, proposals have been considered to load tankers in moving pack ice conditions from offshore terminals. Thus, this topic has important implications in ice engineering for many ice-infested offshore regions.

The data from the Kulluk in the Beaufort Sea are extremely valuable and cover a wide range of ice conditions. However, the results are vessel specific and they do not cover the full range of situations that could be encountered in a moving pack ice scenario. Details concerning the numerical model and comparison with field measurements are presented here.

### **4.2 *Full-Scale Kulluk Data***

The Kulluk had deck and waterline diameters of 100 m and 70 m respectively, an operating draft of 11.5 m, and a displacement of 28,000 tonnes. It had a unique downward sloping circular hull, which failed the oncoming ice in flexure at relatively low force levels. It also had an outward flare near its bottom, to ensure that broken ice pieces cleared around it and did not enter the moonpool or become entangled in the mooring lines (see Figure 11). The vessel had a strong, radially symmetric mooring that, in combination with its circular shape, provided an omni-directional capability to resist ice and storm wave forces. The mooring system was comprised of twelve 0.09 m wire lines and was capable of resisting relatively high ice forces.

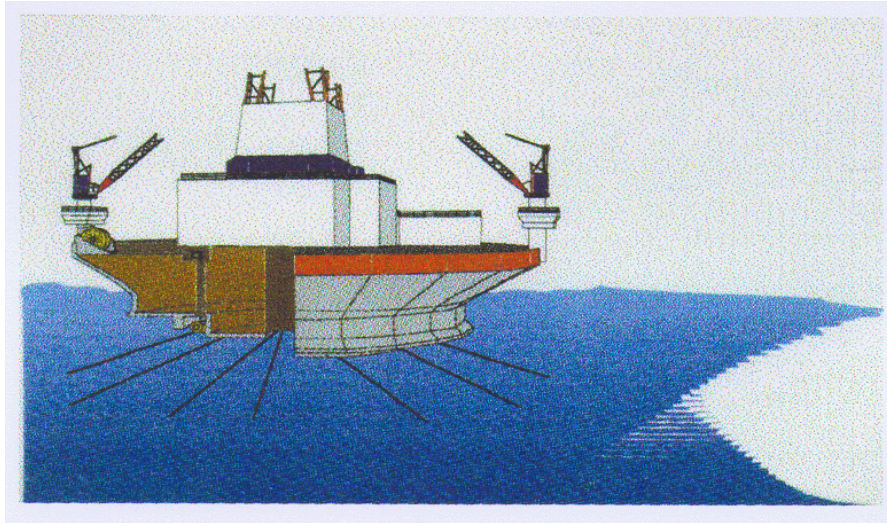
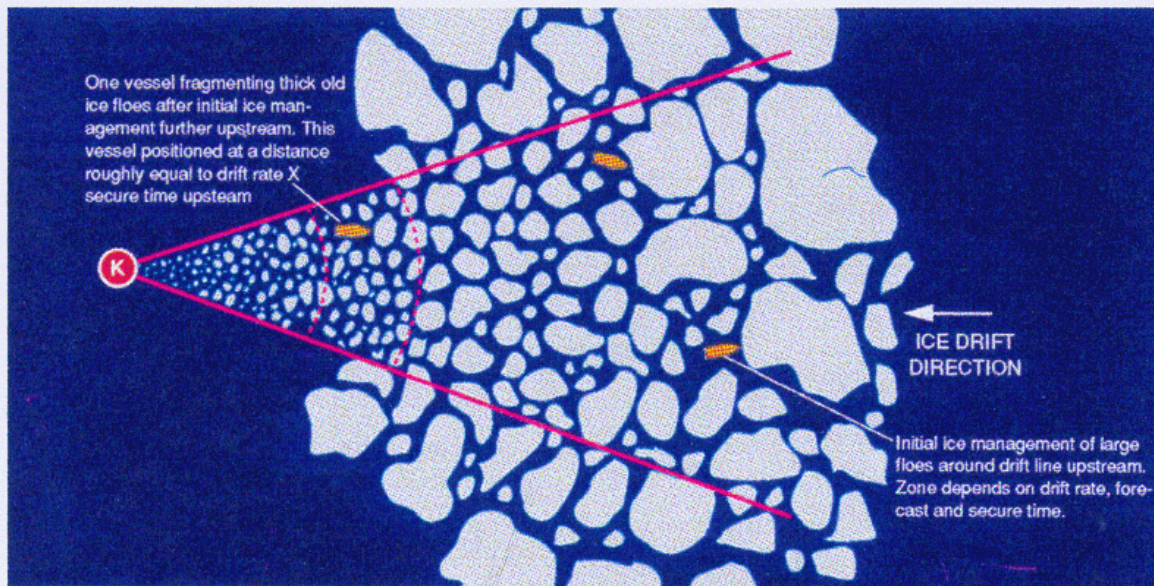


**Figure 11 Illustration of the Kulluk showing its double conical shape and overall features (from Wright, 1999)**

Ice management was a very important factor in enhancing the Kulluk's stationkeeping performance in ice. Typically, several icebreakers supported the Kulluk during its Beaufort Sea operations in heavy pack ice conditions (see Figure 12). These icebreaking vessels broke the ice updrift of the Kulluk into small fragments, which were typically 10 to 30 m in diameter.



### “Picket boat” ice management

Figure 12 The Kulluk and an ice clearing vessel in thick, managed first-year ice conditions and a schematic of one of the ice-clearing techniques (from Wright, 1999)

The loads on the mooring lines were measured during the Kulluk's deployment. Wright (1999) has summarized the loads and categorized them according to the ice conditions. Figure 13 shows a plot of the measured full-scale loads as a function of the ice thickness, for ice concentrations of 0.9 (i.e. 9/10<sup>s</sup> coverage) and higher. Note that, although there is scatter, there is a definite trend of increasing load with increasing thickness. Wright has characterized the upper bound load ( $L_p$ ) as a linear relationship with thickness ( $h$ ) as (see Figure 13):

$$L_p \text{ [MN]} = 0.86h \text{ [m]} + 0.91 \quad (4.1)$$

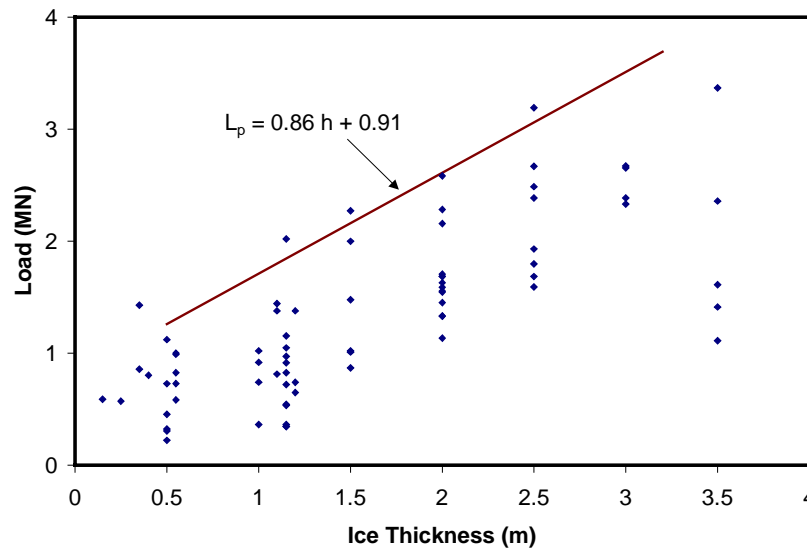


**Figure 13 Measured loads on the Kulluk in tight managed ice with poor clearance and updrift rubble wedge (from Wright, 1999).**

For this sub-set of the data, there was good ice management but relatively poor clearance around the Kulluk. In these situations, there was a “tightness” in the pack ice, which resulted in the formation of an updrift rubble wedge at the structure (see Figure 14).

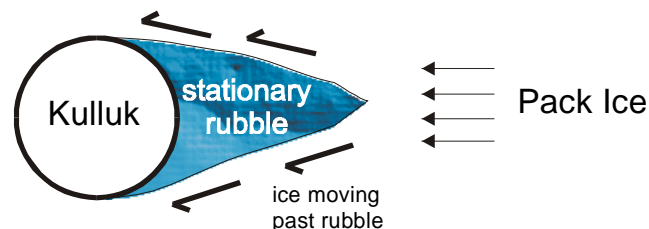


**Figure 14 Schematic of updrift rubble wedge at Kulluk in tight pack ice (after Wright, 1999)**

### 4.3 Base Case for Wide Structure

The numerical grid layout for the Kulluk is shown as a schematic in Figure 15. A 120-by-50-node grid represented the study area, and the grid cell size was set to 10 m. The width of the Kulluk within the grid was therefore 7 nodes. Full slip boundary conditions were once more used at the top and bottom of the grid. In this case, however, if a particle moved through the top boundary, for example, its y-position would be changed to bring it back within the grid at the opposite boundary, again without changing its x-position. A no-slip boundary condition was used for the structure. Velocities of the nodes within the structure were set to zeros. Preliminary tests showed that that this condition produced better agreement with observations than the full-slip condition around the structure.

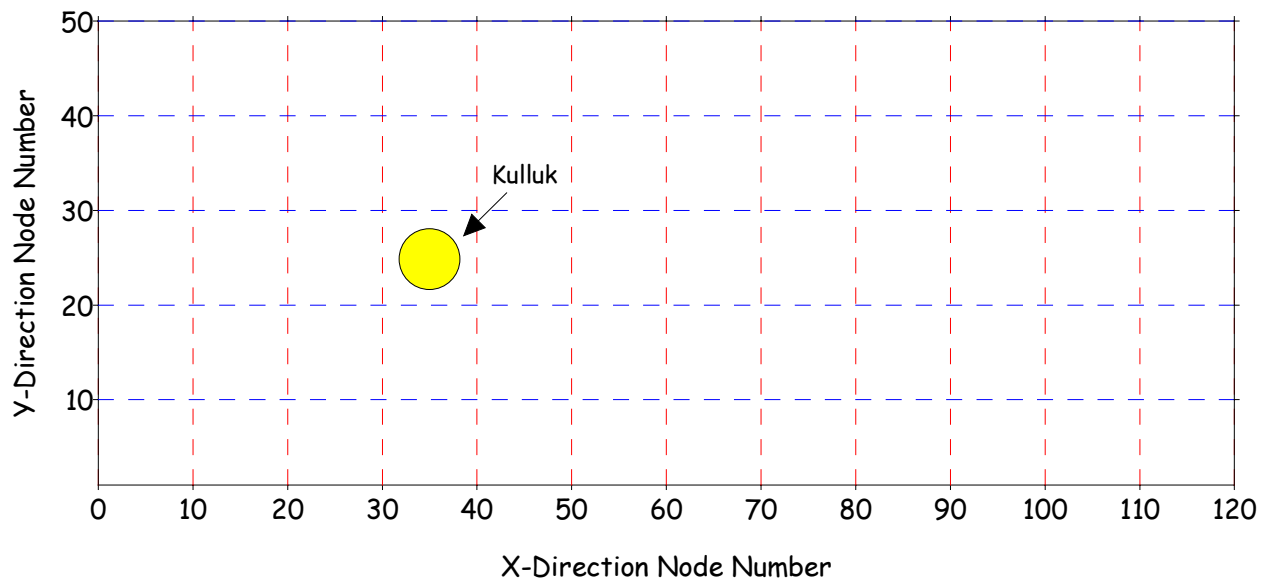


**Figure 15 Base grid for Kulluk modelling**

The ice cover was driven against the Kulluk by imposing a constant velocity upstream, similar to the slender structure model. The constant driving velocity in this case was in a 300 m-wide zone at the upstream side (node numbers 90 to 120 along the x-direction, Figure 15). The grid was initialized with no ice in a 300 m-wide zone at the downstream boundary; hence the ice partially surrounded the Kulluk at the beginning of the program run (see Figure 16).

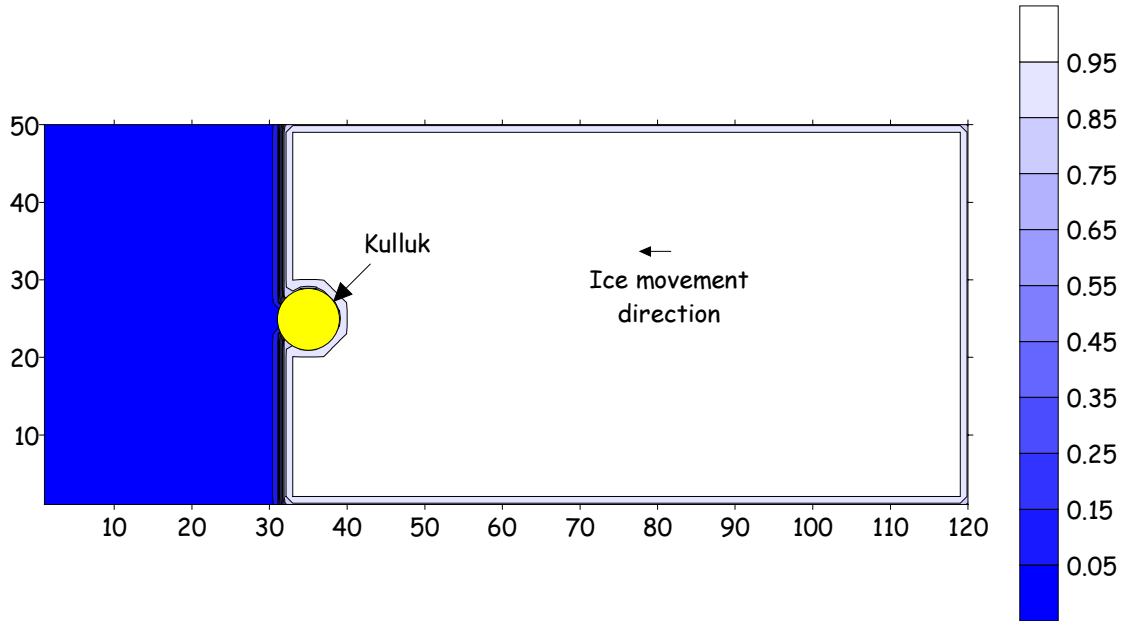


**Figure 16 Initial ice concentration profile around the Kulluk**

For the test cases, records in tight, managed ice were extracted from the original Kulluk database into an Excel spreadsheet. For these cases, there was good ice management but poor clearance around the structure with the formation of a rubble wedge upstream of the structure (see Figure 14).

A base case was selected that had the following properties:

- Ambient ice drift speed = 0.2 m/s
- Ice thickness = 1.5 m
- Local ice concentration = 0.95

The rheology model consisted of a cohesion-less Mohr-Coulomb criterion, and compressibility expressed by Eq. (2.5). Although several laboratory studies have examined the properties of ice rubble, the results cannot be extrapolated to the larger scale of the present ice cover. Therefore, the values of material properties had to be determined by matching the numerical predictions with field observations of a well-documented case from the dataset. Model performance was subsequently tested by comparing predicted peak loads, derived from Wright's equation (Eq. 4.1), to numerical peak loads, using those material properties under a range of conditions.

Runs examined a range of values of the two parameters that determine material properties: the compressibility parameter and the angle of internal friction. From those runs, and previous results (Sayed et al. 2000), a value of 25 kPa for the compressibility parameter,  $P^*$ , was found to produce the appropriate deformation patterns. Note that an excessively low compressibility would produce unrealistically large pileups. Alternatively, a much larger compressibility would prevent any thickness build-up (i.e. no rafting or pileup). The resulting load on the vessel is plotted versus time, for different

values of  $\phi$  in Figure 17. The runs show that a  $\phi$  of  $27^\circ$  results in a good agreement between the predicted and measured peak loads (predicted peak load = 2.27 MN, and measured peak load = 2.20 MN).

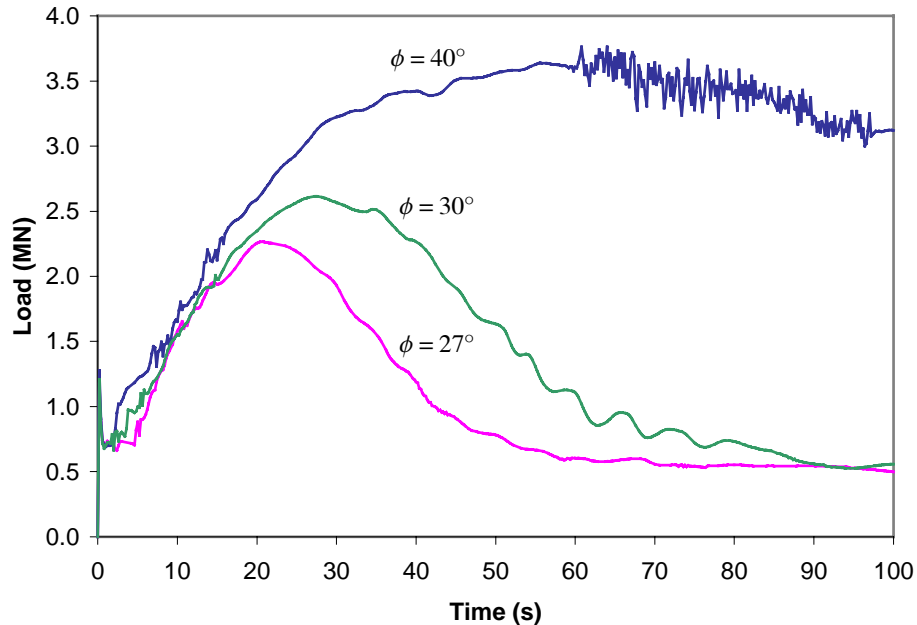


**Figure 17 The effect of  $\phi$  on numerical peak load**

As mentioned previously, a rubble wedge build-up around the Kulluk was experienced in the field (Figure 18). Figure 19 shows two snapshots of the ice concentration around the Kulluk for the base case, 150 and 300 seconds after the start of the run. It can be seen that the resulting wedge from the numerical model is similar to the rubble wedge build up in the field, in terms of approximate size and location. Similar snapshots for pressure and velocity profiles are shown in Figure 20 and Figure 21.

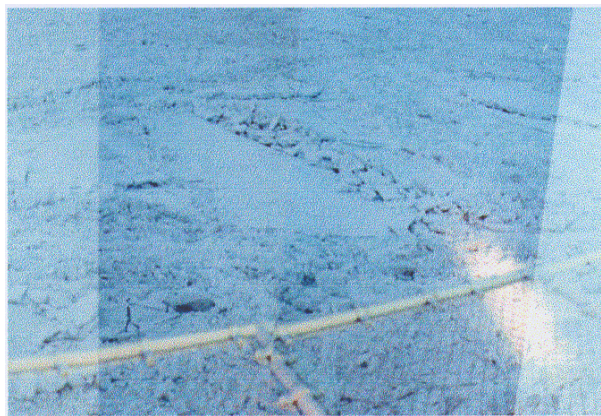


**Figure 18 Rubble wedge build-up in tight pack ice conditions, updrift of the Kulluk (from Wright, 1999)**

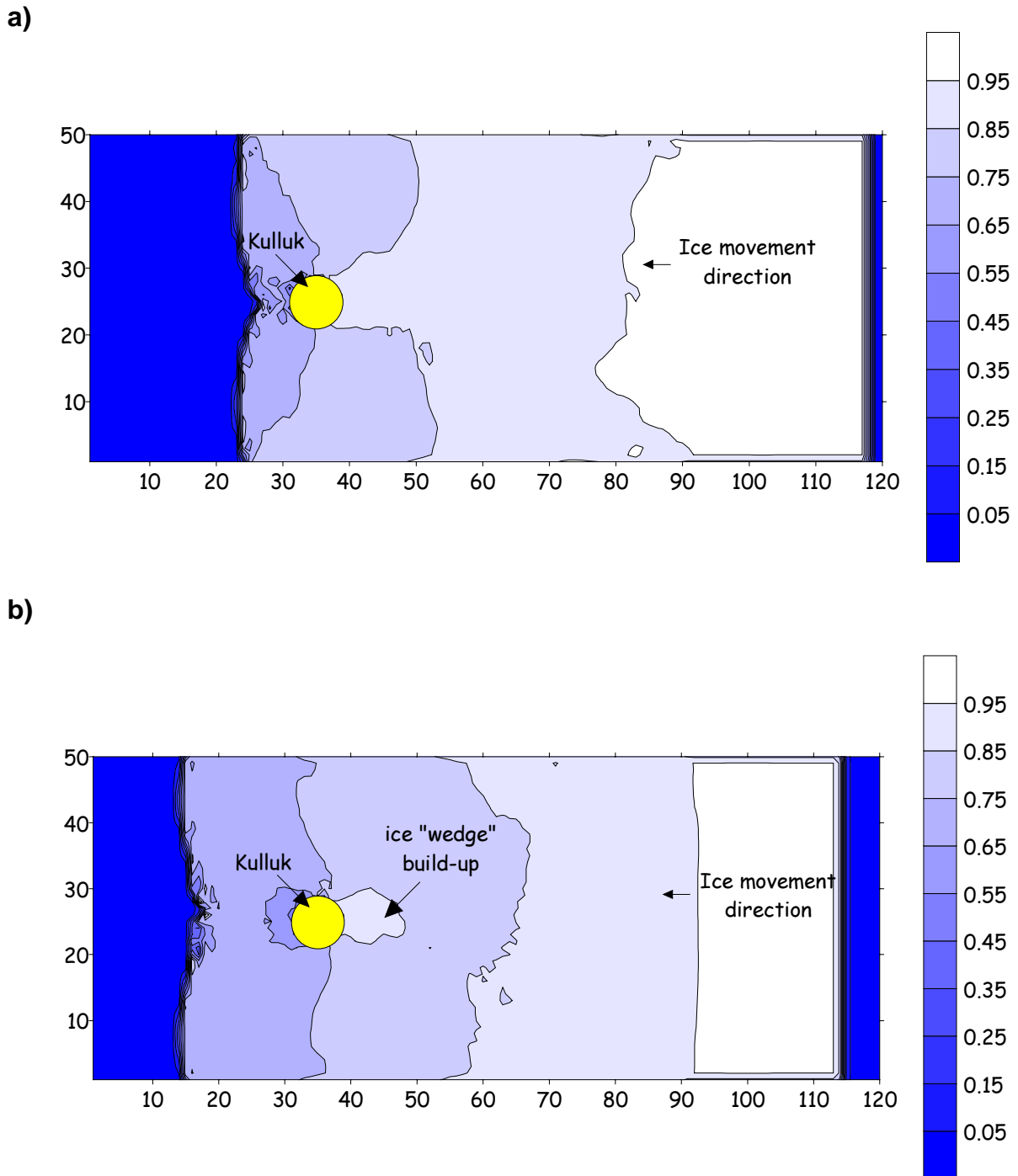


Figure 19 Ice concentration profile around Kulluk showing the ice build-up in front of the Kulluk after a) 150 s and b) 300 s from the start of the run

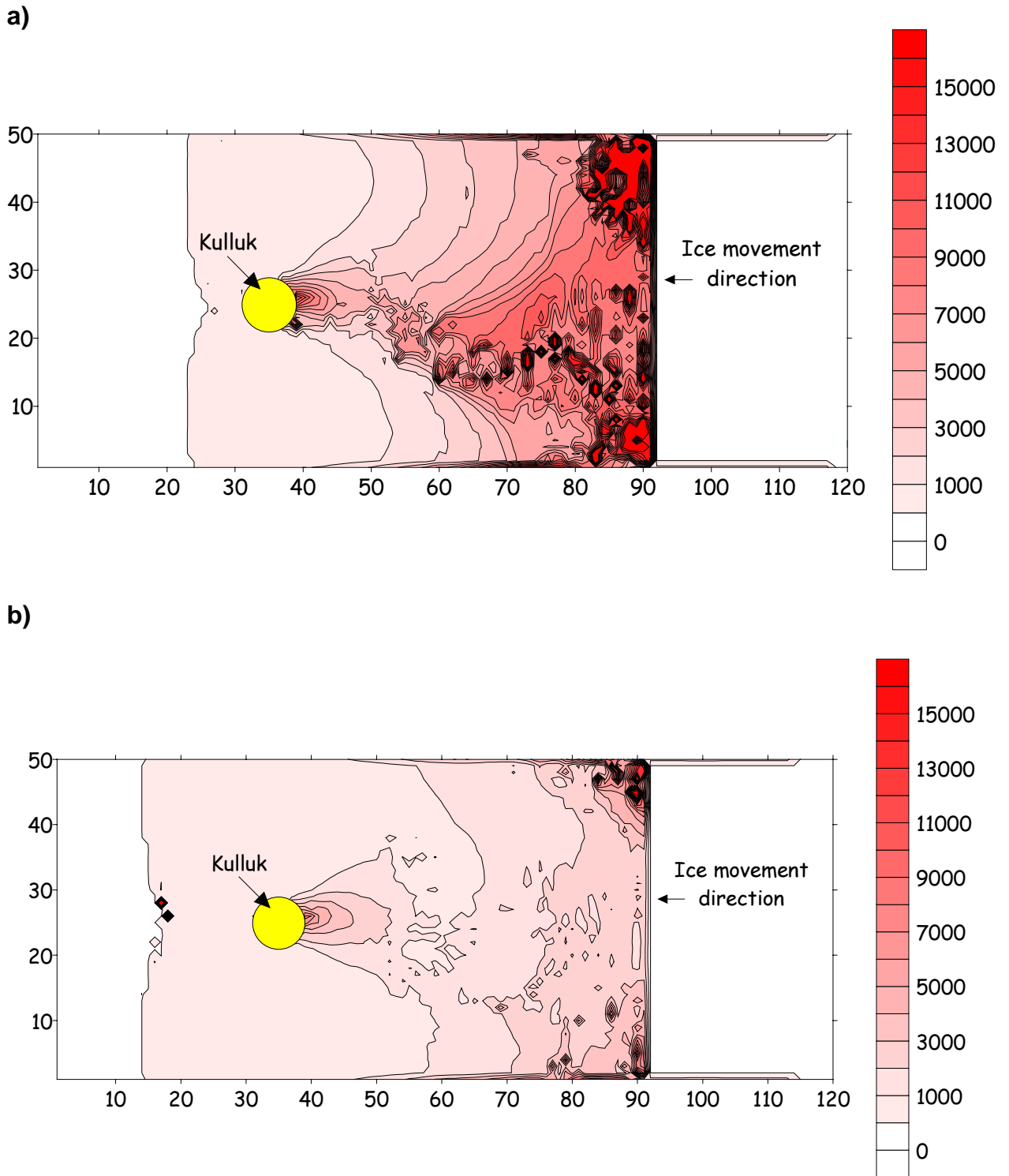
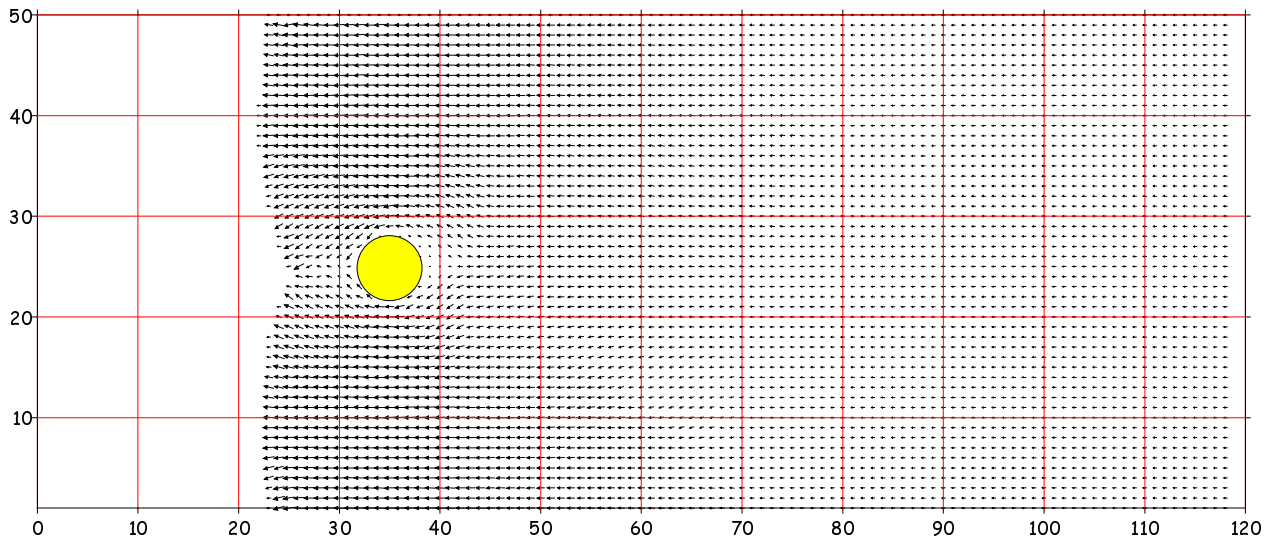
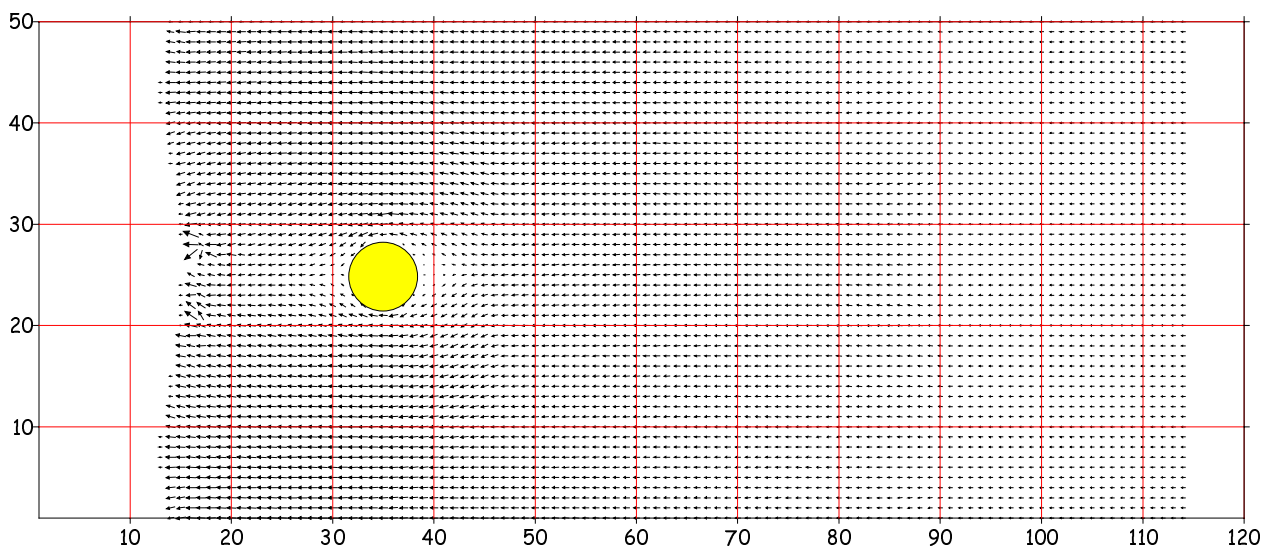


Figure 20 Pressure profiles around the Kulluk after a) 150 s and b) 300 s from the start of the run

a)



b)



**Figure 21 Velocity profiles around the Kulluk after a) 150 s and b) 300 s from the start of the run**

#### 4.4 Parametric Study

Four other representative runs were performed, varying the velocity and thickness parameters, creating a small parametric study. The  $\phi$ ,  $P^*$  and concentration values remained the same throughout these runs. These test runs and their resulting peak loads may be found in Table 4.1.

**Table 4.1 Numerical program input data and peak loads**

	Velocity (m/s)	Thickness (m)	$\phi$ (°)	Concentration	Full-Scale Peak Load (MN)	Numerical Peak Load (MN)
Base case	0.2	1.5	27	0.95	2.20	2.27
Run1	0.2	1.0	27	0.95	1.77	1.52
Run2	0.2	2.0	27	0.95	2.63	3.10
Run3	0.1	1.5	27	0.95	2.20	1.71
Run4	0.3	1.5	27	0.95	2.20	2.58

#### 4.5 Comparison with Measurements and Other Calculation Methods

Figure 22 shows the effects of ice thickness and velocity on the peak numerical load. Also plotted in Figure 22 are the full-scale peak loads for various ice thicknesses from Wright (1999). The numerical peak loads show a linear dependency of load upon thickness, similar to Figure 13. The three data points at  $h=1.5\text{m}$  represent three different velocities. The numerical model also shows a linear dependency upon velocity. It should be noted that the present rheology does not include rate effects. In the present model, velocity effects arise due to the inertia of the pack ice and produce a relationship where load increases with increasing velocity, as one might predict. This dependency is not evident in the full-scale data, over the range of full-scale velocities (Wright, 1999). It should be noted, however, that there was considerable scatter in the full-scale data, and this scatter could have masked any rate effect.

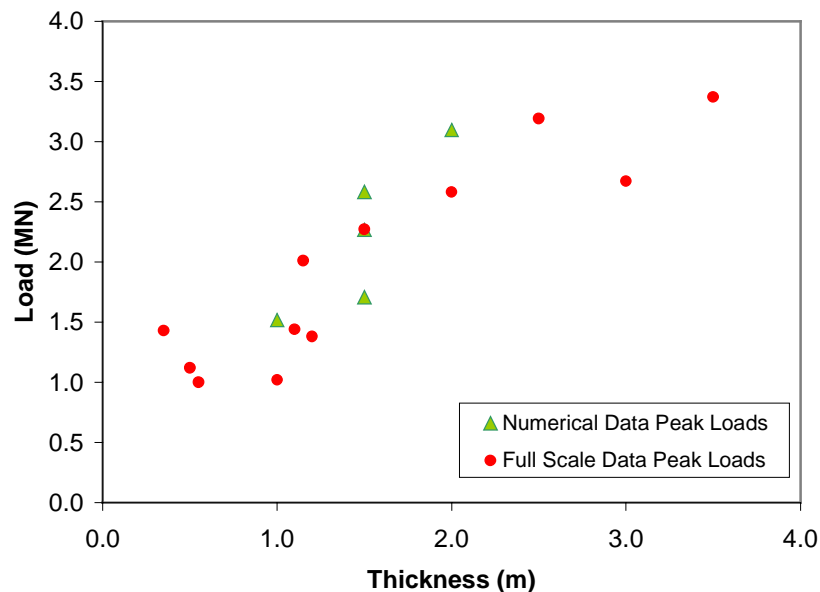


**Figure 22 Numerical load versus initial ice thickness, for  $\phi=27^\circ$ ,  $c=0.95$**

## 5. SUMMARY

Ice forces on slender and wide structures were examined using a numerical model based on a PIC scheme for ice advection and a viscous plastic rheology. For the slender structure model, the model was modified from other versions used for ice forecasting and pack ice interaction with offshore structures. The main modification concerns the introduction of a cohesive Mohr-Coulomb yield criterion.

### ***5.1 Slender Structure in Confined Ice Conditions***

The first simulation addressed the case of rectangular pier with circular front, and ice conditions that corresponded to a well-documented program of field measurements. Those conditions were also chosen because they fall within the range that is commonly encountered (e.g. length scales, and geometry).

The numerical simulations indicate that the model captures the main expected features of ice deformation. For example, the resulting distributions of ice concentration and velocities follow the behaviour observed in the field. The predicted force on the pier was also in agreement with available measurements.

A parametric study showed that cohesion of the ice cover has a large effect on the predicted force. The angle of internal friction had a smaller effect. Tests with different ice velocity showed that velocity has a negligible effect on the force. Slenderness of the pier, which caused only a narrow zone of ice to decelerate, may explain this somewhat unexpected conclusion. It should not be extrapolated, however, for wide structures.

### ***5.2 Wide Structure in Tight, Managed Ice Conditions***

For the second case study, the full-scale data that was examined was obtained from conditions involving tight, managed ice. The upper bound to the peak loads observed at the Kulluk in these conditions is defined by the equation  $L_p=0.86h+0.91$ , as developed by Wright (1999).

The numerical model showed good agreement with the full-scale data. Using  $\phi=27^\circ$ , a linear relationship was observed between thickness and peak load. A linear relationship with ice velocity was found in the numerical data, but not indicated by the full-scale data.

## 6. ACKNOWLEDGEMENTS

The financial support of the Program of Energy Research and Development (PERD), through the ice/structure interaction program, is gratefully acknowledged.

## 7. REFERENCES

- Afanasev, V. 1973. Ice Pressure on Individual Marine Structures. *Ice Physics and Ice Engineering*, G. Yakovlev, Ed., Israel Program for Scientific Translation, pp 50-68.
- Barker, A., Sayed, M. and Timco, G. (2000) Numerical Simulations of Broken Ice Interaction with Structures, PERD/CHC Report HYD-TR-050, Ottawa, Canada.
- Daly, S.F., and Hopkins, M.A. (1998). Simulation of river ice jam formation, *14<sup>th</sup> International Symposium on Ice*, ed. H-T. Shen, Potsdam, USA, Vol. 1, pp. 101-108.
- Ettema, R. and Urroz-Aguirre, G. 1991. Friction and Cohesion in Ice Rubble Reviewed. *Cold Regions Engineering*, pp 316-325, ASME Specialty Conference, West Lebanon, NH, USA.
- Flato, G.M. (1993). A Particle-In-Cell sea-ice model, *Atmosphere-Ocean*, Vol. 31, No. 3, pp. 339-358.
- Hibler, W.D.III (1979). A dynamic thermodynamic sea ice model, *J. Physical Oceanography*, Vol. 9, No. 4, pp. 815-846.
- Johnston, M., Timco, G. and R. Frederking. 1999. An Overview of Ice Load Measurements on Bridge Piers. *Workshop on River Ice*, J. Doering, Ed., pp 290-302, Winnipeg, Manitoba, Canada.
- Korzhasin, K.N. (1971). *Action of ice on engineering structures*, US Army CRREL Translation TL260, Hanover, NH, USA.
- Lu, S., and Shen, H-T. (1998). Constitutive laws for river ice dynamics, *14<sup>th</sup> International Symposium on Ice*, ed. H-T. Shen, Potsdam, USA, Vol. 1, pp. 109-116.
- Sayed, M., and Carrieres, T. (1999). Overview of a new operational ice forecasting model, *ISOPE '99*, Brest, France, Vol. II, pp.622-627.
- Sayed, M., Frederking, R.M.W., and Barker, A. (2000). Numerical simulation of pack ice forces on structures: a parametric study, to appear in *Proceedings of the 10<sup>th</sup> International Offshore and Polar Engineering Conference (ISOPE '2000)*, Seattle, USA, May 28-June 2.
- Sodhi, D., Kato, K. and Haynes, F.D. 1983. *Ice Force Measurements on a Bridge Pier in the Ottawaquechee River, Vermont*. US Army CRREL Report 83-32, Hanover, NH, USA.
- Wright, B. (1999). Evaluation of Full Scale Data for Moored Vessel Stationkeeping in Pack Ice. PERD/CHC Report 26-200, Ottawa, Canada.

Zabilansky, L. 1996. *Ice Force and Scour Instrumentation for the White River, Vermont*. US Army CRREL Special Report 96-6, Hanover, NH, USA.

Zhang, J. and Hibler, W.D.III (1997). On an efficient numerical method for modelling sea ice dynamics, *J. Geophysical Research*, Vol. 102, No. C4, pp. 8691-8702